

## The first-in-class ERK inhibitor ulixertinib shows promising activity in mitogen-activated protein kinase (MAPK)-driven pediatric low-grade glioma models

Romain Sigaud<sup>†</sup>, Lisa Rösch<sup>†</sup>, Charlotte Gatzweiler<sup>†</sup>, Julia Benzel<sup>†</sup>, Laura von Soosten<sup>†</sup>, Heike Peterziel, Florian Selt, Sara Najafi, Simay Ayhan, Xenia F. Gerloff, Nina Hofmann, Isabel Büdenbender, Lukas Schmitt, Kathrin I. Foerster, Jürgen Burhenne, Walter E. Haefeli, Andrey Korshunov, Felix Sahm, Cornelis M. van Tilburg, David T. W. Jones, Stefan M. Pfister, Deborah Knoerzer, Brent L. Kreider, Max Sauter<sup>†</sup>, Kristian W. Pajtler<sup>†</sup>, Marc Zuckermann<sup>†</sup>, Ina Oehme<sup>†</sup>, Olaf Witt<sup>†</sup>, and Till Milde<sup>†</sup>

Hopp Children's Cancer Center Heidelberg (KiTZ), Heidelberg, Germany (R.S., L.R., C.G., J.B., L.vS., H.P., F.S., S.N., S.A., X.F.G., N.H., I.B., L.S., C.M.vT., D.T.W.J., S.M.P., K.W.P., M.Z., I.O., O.W., T.M.); Clinical Cooperation Unit Pediatric Oncology, German Cancer Research Center (DKFZ) and German Consortium for Translational Cancer Research (DKTK), Heidelberg, Germany (R.S., L.R., C.G., H.P., F.S., S.N., S.A., X.F.G., I.B., C.M.vT., I.O., O.W., T.M.); Faculty of Biosciences, Heidelberg University, Heidelberg, Germany (L.R., J.B., L.vS., S.A.); Faculty of Medicine, Heidelberg University, Heidelberg, Germany (C.G.); Division of Pediatric Neurooncology, German Cancer Consortium (DKTK), German Cancer Research Center (DKFZ), Heidelberg, Germany (J.B., S.M.P., K.W.P.); Preclinical Modeling Group, German Cancer Research Center (DKFZ), Heidelberg, Germany (L.vS., N.H., M.Z.); Division of Pediatric Glioma Research, German Cancer Research Center (DKFZ), Heidelberg, Germany (L.vS., D.T.W.J.); KiTZ Clinical Trial Unit, Department of Pediatric Oncology, Hematology, Immunology and Pulmonology, Heidelberg University Hospital, Heidelberg, Germany (F.S., S.N., S.A., X.F.G., C.M.vT., S.M.P., K.W.P., O.W., T.M.); Pediatric Soft Tissue Sarcoma Research Group, German Cancer Research Center (DKFZ), Heidelberg, Germany (L.S.); Department of Clinical Pharmacology and Pharmacoepidemiology, Heidelberg University Hospital, Heidelberg, Germany (K.I.F., J.B., W.E.H., M.S.); Department of Neuropathology, Heidelberg University Hospital, Heidelberg, Germany (A.K., F.S.); Clinical Cooperation Unit Neuropathology, German Consortium for Translational Cancer Research (DKTK), German Cancer Research Center (DKFZ), Heidelberg, Germany (A.K., F.S.); BioMed Valley Discoveries Inc., Kansas City, Missouri, USA (D.K., B.K.)

**Corresponding Author:** Till Milde, MD, Hopp Children's Cancer Center Heidelberg (KiTZ), Im Neuenheimer Feld 280, Heidelberg 69120, Germany (t.milde@kitz-heidelberg.de).

<sup>†</sup>These authors contributed equally to this work.

### Abstract

**Background.** Pediatric low-grade gliomas (pLGG) are the most common pediatric central nervous system tumors, with driving alterations typically occurring in the MAPK pathway. The ERK1/2 inhibitor ulixertinib (BVD-523) has shown promising responses in adult patients with mitogen-activated protein kinase (MAPK)-driven solid tumors.

**Methods.** We investigated the antitumoral activity of ulixertinib monotherapy as well as in combination with MEK inhibitors (MEKi), BH3-mimetics, or chemotherapy in pLGG. Patient-derived pLGG models reflecting the two most common alterations in the disease, *KIAA1549:BRAF*-fusion and *BRAF*<sup>V600E</sup> mutation (DKFZ-BT66 and BT40, respectively) were used for in vitro and in vivo (zebrafish embryos and mice) efficacy testing.

**Results.** Ulixertinib inhibited MAPK pathway activity in both models, and reduced cell viability in BT40 with clinically achievable concentrations in the low nanomolar range. Combination treatment of ulixertinib with MEKi or BH3-mimetics showed strong evidence of antiproliferative synergy in vitro. Ulixertinib showed on-target activity in all tested combinations. In vivo, sufficient penetrance of the drug into brain tumor tissue in concentrations above the in vitro IC<sub>50</sub> and reduction of MAPK pathway activity was achieved. In a preclinical mouse trial, ulixertinib mono- and combined therapies slowed tumor growth and increased survival.

**Conclusions.** These data indicate a high clinical potential of ulixertinib for the treatment of pLGG and strongly support its first clinical evaluation in pLGG as single agent and in combination therapy in a currently planned international phase I/II umbrella trial.

### Key Points

- The ERKi ulixertinib is active in pLGG models in clinically achievable concentrations.
- Ulixertinib combination with MEK inhibitors or BH3-mimetics are synergistic in vitro.
- Ulixertinib significantly increased survival in BT40-PDX mouse model in vivo.

### Importance of the Study

Despite excellent overall survival rates, pediatric low-grade glioma (pLGG) patients are at high risk of recurrence, and often suffer from extensive disease- and therapy-related morbidity. Complete resection is not always possible, and chemo-/radiotherapy fail to achieve complete remission, resulting in only partial response or stable disease. Thus, new therapeutic approaches are urgently needed. BRAF and MEK inhibitors are in clinical evaluation and show promising first results. However, variable responses to and rebound-growth after treatment with MAPKi remain clinical challenges,

necessitating investigation of new compounds. We here present the first preclinical evidence for antitumoral efficacy of the first-in-class ERK inhibitor ulixertinib in pLGG in vitro and in vivo, significantly increasing mouse survival. Additionally, the synergistic combinations of ulixertinib with MEKi or BH3-mimetics warrant further exploration. These comprehensive preclinical data will support the first clinical evaluation of an ERKi for the treatment of pLGG in an international phase I/II umbrella trial.

Pediatric low-grade glioma (pLGG) is the most common pediatric central nervous system (CNS) tumor.<sup>1</sup> Its treatment remains a challenge, mainly because of the associated chronic morbidity. Despite a favorable 10- and 20-year overall survival (OS) of 87% and 82%, respectively, overall 10-year progression-free survival (PFS) remains low with 58%,<sup>2</sup> and patients with recurring disease often need multiple treatments. The preferred treatment is surgical resection,<sup>3</sup> the efficacy of which is a major determinant of PFS, with a 10-year PFS of 82% after gross total resection vs 48% after sub-total resection.<sup>2</sup> Additional standard of care (SOC) therapeutic modalities are chemotherapy (carboplatin/vincristine,<sup>4</sup> or vinblastine<sup>5</sup>) and radiotherapy. Chemotherapy has shown clinical benefit, but the effects are more pronounced in patients with NF1-driven pLGG (3-year PFS 80% or 92% for carboplatin/vincristine, or vinblastine, respectively) compared to non-NF1-driven pLGG (3-year PFS 55% or 56%).<sup>4,5</sup> Thus, novel effective systemic treatments are needed.

pLGG is considered a single-pathway disease, with most driving alterations occurring in the mitogen-activated protein kinase (MAPK) pathway<sup>6</sup> (most frequently *KIAA1549:BRAF*-fusion,<sup>7</sup> *BRAF*<sup>V600E</sup> mutation,<sup>8</sup> *FGFR1* alterations,<sup>8</sup> and *NF1* mutations<sup>8</sup>), leading to oncogene-induced senescence.<sup>9,10</sup> Consequently, MAPK inhibitors (MAPKi), such as the MEK inhibitors (MEKi) selumetinib,<sup>11</sup>

trametinib (NCT02124772) and binimetinib,<sup>12</sup> and the BRAF inhibitors (BRAFi) dabrafenib<sup>13</sup> and vemurafenib,<sup>14</sup> have shown encouraging results in clinical trials. MAPKi treatment induced a stable disease (SD) in most cases, and objective response rates of 30–54% only were achieved.<sup>11–14</sup> As with chemotherapy however, these therapies are frequently accompanied by side effects, leading to treatment cessation,<sup>3</sup> often followed by tumor growth rebound.<sup>11,13,15</sup> Therefore, additional approaches are required to improve the treatment's efficacy in pLGG.

The MAPK pathway comprises three core nodes in what is usually thought of as a linear process: BRAF, MEK, and ERK.<sup>16</sup> While BRAF and MEK have few direct downstream targets, ERK represents the pathway's hub, with more than 150 cytosolic and nuclear downstream phosphorylation targets.<sup>17</sup> Its ability to localize in many cellular compartments upon activation makes it a key player in the regulation of several cancer mechanisms.<sup>18</sup> ERK is also involved in negative feedback loops regulating the MAPK pathway on the level of RAF,<sup>19</sup> potentially enabling MAPK pathway reactivation after indirect inhibition by BRAFi or MEKi. Hence, direct targeting of ERK represents a different, novel, and promising approach for the treatment of MAPK-driven tumors.

Ulixertinib (BVD-523), a reversible, ATP-competitive, catalytic ERK1/2 inhibitor, is an orally administered

drug with an acceptable safety profile,<sup>20</sup> with promising preclinical antitumoral activity in MAPK-driven adult tumors in vitro and in vivo.<sup>21,22</sup> Ulixertinib is currently being tested in a clinical phase II trial with pediatric patients with MAPK pathway mutations (NCT03698994), and pediatric patients with relapsed solid and brain tumors (NCT03155620). Its activity in pLGG however remains unknown.

Ulixertinib has shown antitumoral synergy preclinically when used in combination with BRAFi in BRAF-mutant-driven melanoma models.<sup>22</sup> Other drugs for potential combination with ulixertinib in pLGG are 1) MEKi, because targeting the MAPK pathway on two different nodes has demonstrated synergism in vitro in pLGG models,<sup>23</sup> and clinical efficacy (NCT02124772), and could avoid the reactivation of the MAPK pathway after ERK inhibition; 2) BH3-mimetics, because they target senescent pLGG cells in vitro,<sup>24</sup> as well as proliferating pLGG cells after initiation of therapy-induced senescence by MAPKi pretreatment<sup>25</sup>; and 3) chemotherapy, the current SOC for pLGG.

Here, we generated an extensive preclinical dataset to evaluate the potential of ulixertinib for clinical development in BRAF-driven pLGG patients. Ulixertinib was studied as mono- and combination-therapy with MEKi, BH3-mimetics, and chemotherapy, including in vitro and in vivo experiments.

## Materials and Methods

### Cell Culture

The pilocytic astrocytoma cell line (DKFZ-BT66; *KIAA1549:BRAF*-fusion) was cultured in its proliferative and senescent mode, as described.<sup>10</sup> The pleomorphic xanthoastrocytoma cell line<sup>26</sup> (BT40; BRAF<sup>V600E</sup> mutation and CDKN2A del; kindly provided by Prof. Houghton) was grown as described.<sup>10,23,24</sup> DKFZ-BT66 and BT40 transduced with a MAPK reporter construct (pDIPZ) were cultured as described.<sup>23</sup>

### Drug Treatments In Vitro

All experiments (unless stated otherwise) were performed in 384-well plates (Cat#3570, Corning). Metabolic activity measurement was performed after 72 h drug treatment, and luciferase activity after 24 h drug treatment, as described.<sup>23</sup> For IC<sub>50</sub> calculations see Supplementary Methods.

### High Content Microscopy

Cells were seeded as indicated (Supplementary Table S1), treated for 72 h after five days, stained at room temperature for 20 min as indicated in Supplementary Table S2, and imaged with an ImageXpress Micro Confocal high content microscope (Molecular Devices). Image analysis was performed with Cell Profiler Version 5.<sup>27</sup> For details, see Supplementary Methods.

### Synergy Analysis

A 5 × 5 matrix design and a ray design<sup>28</sup> with seven rays were used to measure synergy metrics (synergy scores, CSS), as indicated (Supplementary Table S3). Synergy was assessed using the Loewe, Bliss independence, or highest single agent (HSA) model.<sup>29</sup> For details on the choice of the synergy model, see Supplementary Methods.

### In Vitro On-target Activity Validation

For ulixertinib on-target activity, cells were seeded in 6-well plates and treated for 24 h with the corresponding drugs. For navitoclax on-target activity, cells were seeded in 10 cm dishes and treated for 4 h, as indicated. Samples were harvested, as described in Supplementary Methods.

### Western Blot and Immunoprecipitation

Western blot analysis was performed as described.<sup>23</sup> Immunoprecipitation was done using Dynabeads™ Protein G Immunoprecipitation Kit (Invitrogen 10007D) following the manufacturer's instructions. For antibodies used, see Supplementary Table S4.

### Reverse Phase Protein Array

Reverse-phase protein array (RPPA) was conducted at Theralink®, as described.<sup>30,31</sup> For antibodies used, see Supplementary Table S5. Raw values were first normalized to beta-actin and then to DMSO control. Markers showing high coefficients of variation across replicates or discrepancies in positive controls were excluded (Supplementary Figure S1).

### Zebrafish Embryo Toxicity Assay, Xenotransplantation, and Treatment

AB strain wild-type zebrafish embryos were used. Breeding and husbandry of zebrafish, and embryo culture were done as described.<sup>32</sup> For toxicity assay see Supplementary Methods. BT40 cells were labeled with CellTracker CM-Dil (Cat#C7000; Thermo Fisher Scientific). DKFZ-BT66\_ON and DKFZ-BT66\_OFF cells stably express RFP. Cell injection was done as previously described,<sup>32</sup> at 48 h post fertilization using 8–10 µl of cell suspension (approx. 150–200 cells). For xenograft imaging and treatment, see Supplementary Methods.

### BT40 Xenograft Mouse Model, Treatment, and Imaging

Six to seven weeks old female NSG (NOD.Cg-Prkdc<sup>scid</sup>Il2rg<sup>tm1Wjl</sup>/SzJ—NOD SCID gamma mice) (Charles River, internal breeding) mice were used. Prior to injection, BT40 cells were transduced with a lentiviral luciferase reporter (pGreenFire1, Cat#TR010PA-1, SBI System Biosciences). Subsequently, cells (1.8–2.0 × 10<sup>5</sup> in 4 µl media) were intracranially transplanted into the cortex

(pharmacokinetic study: ML -1, AP -1, DV -1.5; preclinical study: ML -1, AP 1, DV -1.5). For bioluminescence measurements, VivoGlo™ luciferin-solution (150 mg/kg; Cat#7903, BioVision) was injected intraperitoneally 10 min prior to imaging using the In Vivo Imaging System (IVIS) Lumina Series III (Caliper Life Sciences).

### Pharmacokinetic Study

BT40 cells were injected ( $n = 56$  mice) and tumor growth was verified by IVIS. The single dose cohort ( $n = 28$ ) received one oral application of 80 mg/kg ulixertinib in 0.25 ml per 25 g mouse. The multiple dose cohort ( $n = 28$ ) was dosed twice daily (every 12 h) for five consecutive days. The pharmacokinetic study lasted 24 h after the last injection. For sample processing see Supplementary Materials.

### Ulixertinib and Navitoclax Bioanalysis

Ulixertinib and navitoclax concentrations were analyzed using validated UPLC-MS/MS quantification assays (Supplementary Materials). Ulixertinib on-target activity was assessed in tissue samples (healthy tissue and tumor tissue) from each time point from both cohorts as described in Supplementary Material.

### In Vivo Preclinical Study

After orthotopic transplantation of BT40 cells into 48 NSG mice within two days (24 mice/day), tumors were allowed to develop for two weeks. The groups were randomly assigned to the following treatments: navitoclax (A), ulixertinib + navitoclax (B), ulixertinib + vinblastine (C), vehicle (D), vinblastine (E), ulixertinib (F), for application and dosing, see Supplementary Materials. The continuous 19-day-treatment started three days after group distribution. The observation period with bi-weekly bioluminescence imaging started after reaching the average 35.5 days latency of the model (occurrence of termination criteria due to tumor growth). All animal experiments were conducted in accordance with the local animal welfare regulations and have been approved by the responsible authorities (Regierungspräsidium Karlsruhe, Germany, approval number G-76/20).

### Statistical Analysis and Graphical Representations

For details, see Supplementary Materials.

## Results

### *Ulixertinib is Active in Clinically Achievable Concentrations in BRAF<sup>V600E</sup> Mutant and KIAA1549:BRAF-Fusion Cell Lines*

To investigate the antitumoral activity of ulixertinib in vitro, we used the BRAF<sup>V600E</sup> mutant model “BT40” (proliferating

cells), and the *KIAA1549:BRAF*-fusion model “DKFZ-BT66”, both in its proliferating (DKFZ-BT66\_ON) and senescent mode (DKFZ-BT66\_OFF), as described.<sup>10</sup> In BT40, ulixertinib reduced metabolic activity at clinically achievable concentrations, with an IC<sub>50</sub> of 62.7 nM (Figure 1A). Notably, compared to the IC<sub>50</sub> values derived from 761 cancer cell lines in the Genomics of Drug Sensitivity in Cancer (GDSC) study,<sup>33</sup> the metabolic IC<sub>50</sub> in BT40 cells was remarkably low under the same treatment conditions (Figure 1G). Importantly, ulixertinib sensitivity was associated with BRAF-driving alterations in the pan-cancer dataset (Figure 1H), and in its glioma subset (Figure 1I). Ulixertinib did not affect metabolic activity in DKFZ-BT66 proliferating (Figure 1B) or senescent (Figure 1C) cells, as previously observed with various MAPK inhibitors.<sup>10,23</sup> We used a MAPK reporter assay<sup>23</sup> to assess ulixertinib potency, and showed a complete inhibition of the MAPK pathway in all three cell lines with IC<sub>50</sub> of ~10 nM (Figure 1D–F). Taken together, these data indicate that ulixertinib is active in a clinically achievable nanomolar range in both BRAF<sup>V600E</sup> mutant and *KIAA1549:BRAF*-fusion pLGG cells.

### *Ulixertinib Acts Synergistically in Combination with MEKi and BH3-Mimetics In Vitro*

We investigated potential antitumoral effects of ulixertinib in combination with MEK inhibitors (MEKi—binimetinib, selumetinib, trametinib), BH3-mimetics (A-1331852, navitoclax, venetoclax), and SOC chemotherapy (carboplatin, vinblastine). Metabolic IC<sub>50</sub> was reached in clinically achievable concentrations with all single drugs except venetoclax and carboplatin (Supplementary Figure S2A; Supplementary Table S6). Of note, all BH3-mimetics had lower IC<sub>50</sub> in the senescent pLGG cells compared to their proliferative counterpart, validating BH3-mimetics sensitivity dependency towards cell's senescent priming rather than the MAPK pathway alteration status. The MAPK activity IC<sub>50</sub> was also measured (Supplementary Figure S2B; Supplementary Table S6), and showed MEKi-induced inhibition of the MAPK pathway in the nanomolar range.

In the BRAF<sup>V600E</sup> mutant model, the combinations of ulixertinib with trametinib, binimetinib, or A-1331852 showed synergy or additivity for most rays tested (Figure 2A). Synergy scores in the matrix design ranged from synergy to additivity with a tendency towards buffering antagonism (i.e. when one drug masks the effect of the other) (Figure 2A). Increased drug sensitivity was also observed (Figure 2A, Supplementary Figures S3 and S4A). The synergistic interaction in the combination with binimetinib was observed with the MAPK reporter assay (Figure 2B, Supplementary Figures S5 and S6).

In the proliferating *KIAA1549:BRAF*-fusion model, synergy scores suggested synergy for the combination with BH3-mimetics (Figure 2C, Supplementary Figures S3 and S4B). Venetoclax showed the highest synergy scores, however, in concentrations higher than clinically achievable. The combinations with chemotherapy showed overall buffering antagonism (Figure 2C, Supplementary Figures S3 and S4B). The combinations with binimetinib and trametinib showed strong synergism, while the combination with selumetinib showed buffering antagonism (Figure 2D, Supplementary Figures S5 and S6).

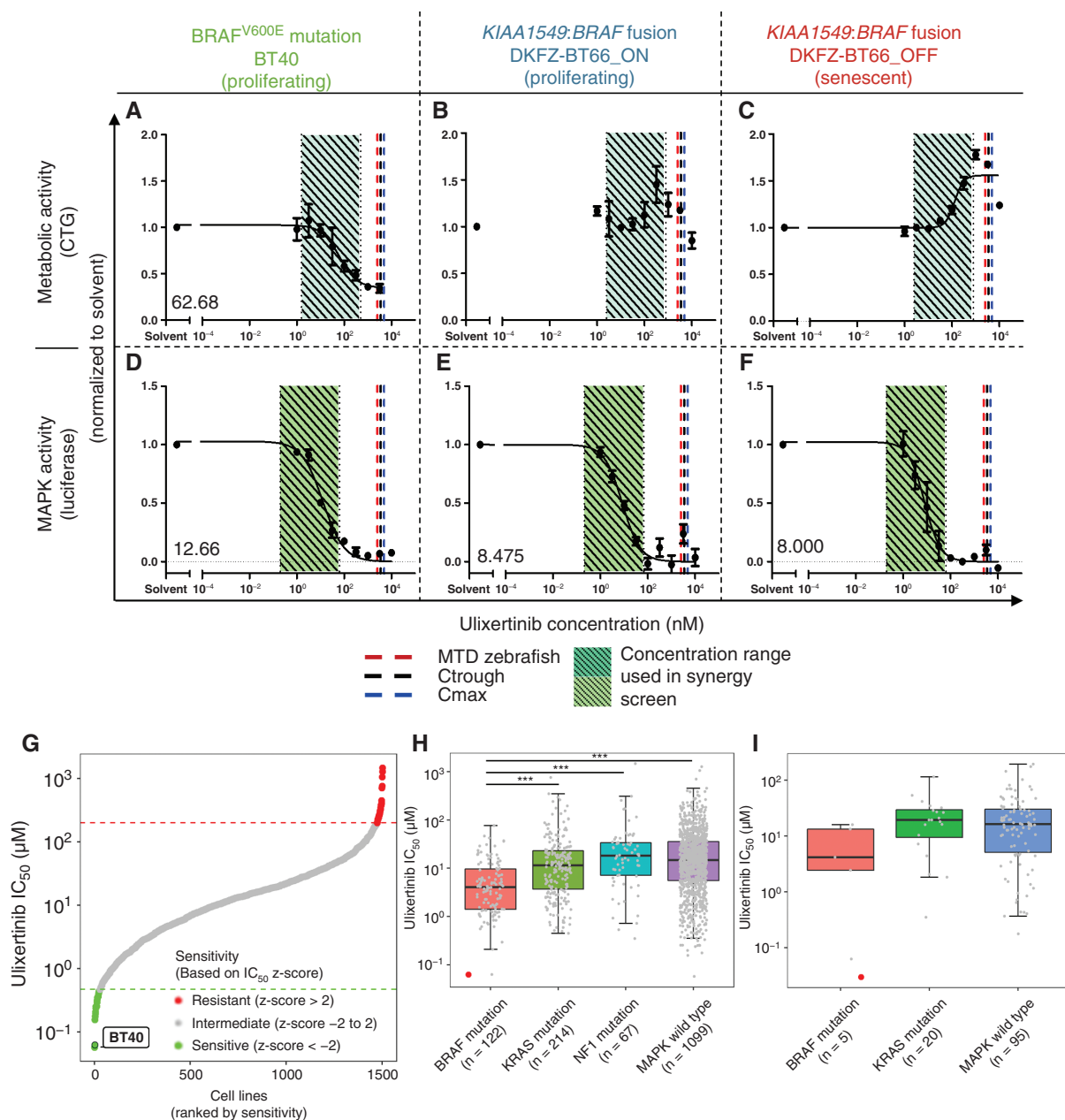


**Fig. 1** Ulixertinib activity in vitro in BRAF<sup>V600E</sup> mutant and KIAA1549:BRF-fusion pLGG cell lines. (A), (B), and (C) Metabolic activity IC<sub>50</sub> measured in BT40 (A), DKFZ-BT66\_ON (B), and DKFZ-BT66\_OFF (C); (D), (E), and (F) MAPK reporter IC<sub>50</sub> measured in BT40 (D), DKFZ-BT66\_ON (E), and DKFZ-BT66\_OFF (F); mean ± standard deviation of three independent biological replicates. Cmax, maximum concentration; Cthrough, trough concentration; MTD, maximum tolerated dose. (G) Summary of IC<sub>50</sub> from the GDSC database and BT40 IC<sub>50</sub>. (H) Boxplot depicting ulixertinib's IC<sub>50</sub> in all pan-cancer cell lines included in the GDSC dataset. (I) Boxplot depicting ulixertinib's IC<sub>50</sub> in glioma cell lines only from the GDSC dataset (highlighted dot = BT40).

In the senescent KIAA1549:BRF-fusion model, combinations with BH3-mimetics showed synergy, with best results obtained in combination with navitoclax or A-1331852 (Figure 2E, Supplementary Figures S3 and S4C). The combinations with chemotherapy showed additivity with tendency towards buffering antagonism (Figure 2E, Supplementary Figures S3 and S4C). The combinations

with binimetinib and trametinib had the highest synergy scores (Figure 2F, Supplementary Figures S5 and S6).

Consensus ranking of all class-related drugs based on their synergy scores (Supplementary Figure S7), followed by a ranking across all readouts, identified the MEKi binimetinib and trametinib, and the BH3-mimetics navitoclax and A-1331852 as best combination partners

(Figure 2G). Amongst the chemotherapeutics, carboplatin had the best consensus ranking. However, its poor clinical profile<sup>34</sup> and its IC<sub>50</sub> out of clinical relevance in our models made vinblastine the overall best combination partner among the chemotherapeutic agents. Additionally, A-1331852 is currently not being evaluated clinically. A-1331852 and carboplatin were excluded to focus on clinically relevant data.

### Ulixertinib Shows On-target Activity in Combinations With MEKi, BH3-Mimetics, or Chemotherapy In Vitro

We investigated ulixertinib's on-target activity in combination with a MEKi (trametinib), a BH3-mimetic (navitoclax), or chemotherapy (vinblastine), as a proof-of-concept. Phospho-ERK cannot be used as a direct readout to assess ulixertinib on-target activity.<sup>22</sup> Instead, several downstream ERK targets were investigated via RPPA and Western blot (Figure 2H). Samples treated with ulixertinib showed differential phosphorylation of ERK targets compared to untreated samples (Supplementary Figure S8A), and a ulixertinib dose-dependent effect was observed in all combinations (Supplementary Figure S8B–D). Taken together, our data showed a dose-dependent inhibition of ERK target phosphorylation, indicating on-target activity in all investigated combinations.

On-target activity of BH3-mimetics at working doses (i.e. respective IC<sub>50</sub>) was also confirmed in all models (Supplementary Figure S9).

### High Content Microscopy Validates Binimetinib and Navitoclax as Effective Combination Partners for Ulixertinib In Vitro

In BT40, single treatments with ulixertinib, MEK inhibitors, navitoclax, and vinblastine decreased cell number and viability. Apoptosis was detected upon single treatment with trametinib, binimetinib, and navitoclax, with the strongest apoptosis induction observed in the treatment with navitoclax (Supplementary Figure S10A–B). Scores suggesting synergistic reduction of cell proliferation (Figure 3A and Supplementary Figure S11A) and viability (Figure 3B and Supplementary Figure S11B) were measured in the combinations of ulixertinib with binimetinib, selumetinib, and vinblastine. The combinations with binimetinib and navitoclax showed synergistic effects on cell death (Figure 3C and Supplementary Figure S11C). Particularly, the combinations with binimetinib, trametinib, navitoclax, and vinblastine induced apoptosis in a synergistic manner (Figure 3D and Supplementary Figure S11D).

In DKFZ-BT66, single treatment with BH3-mimetics decreased cell number and increased cell death in both proliferating and senescent modes. Single chemotherapy treatment inhibited proliferation and induced cell death in the proliferating cells, while having no effect on the senescent cells. All MAPKi, used as single agents, did not induce cell death in either proliferating or senescent modes. While MAPKi did not alter cell numbers in the proliferating model, they increased cell number in the senescent model,

associated with an increase of cell size (Supplementary Figure S12A–C). Scores suggesting antagonism on the proliferation and cell size levels were found in all combinations tested in both proliferating and senescent cells (Figure 3E–H, and Supplementary Figure S13A–D). The effects on induction of cell death were additive at best (Figure 3I and J, and Supplementary Figure S13E–F).

Consensus ranking of all drugs based on their synergy scores (Supplementary Figure S14), followed by a ranking across all readouts, identified binimetinib, navitoclax, and vinblastine as best combination partners for ulixertinib overall (Figure 3K).

### A Zebrafish Embryo Study Validates Navitoclax and Binimetinib as Effective Combination Partners for Ulixertinib In Vivo

To date, the zebrafish embryo model represents the only alternative to study senescent pLGG in vivo. Noninjected zebrafish embryos were treated as indicated to determine the respective maximum tolerated dose (MTD) and lethal dose (LD) (Figure 4A, Supplementary Table S6). Ulixertinib was well tolerated by the zebrafish embryo up to 2.5 μM. Tumor growth in pLGG xenografts upon treatment was evaluated based on progressive disease over partial response (PD/PR) ratio (Figure 4B and Supplementary Figure S15). Only in the proliferating DKFZ-BT66\_ON xenografts did ulixertinib alone achieve a PD/PR ratio < 1.0 (Figure 4C). In all other models, this effect was only achieved with combination treatments, substantially increasing treatment response compared to single treatments. The combination with navitoclax led to the best partial response rate compared to the combination with binimetinib in all three models (BT40 54% vs. 33%; DKFZ-BT66\_ON 67% vs. 36%; DKFZ-BT66\_OFF 23% vs. 22%) (Supplementary Figure S16A–C). These data identify navitoclax as a promising combination partner for ulixertinib to inhibit BRAF-driven pLGG tumor growth to be further validated in vivo.

### Ulixertinib Toxicity, Pharmacokinetic, and Pharmacodynamic In Vivo Studies in Mice

The treatment of NSG mice twice daily for five consecutive days with ulixertinib was not associated with weight loss, as a surrogate for toxicity (Supplementary Figure S17A). The average weight change after ulixertinib treatment was  $-1.67 \pm 5.84\%$  (Supplementary Figure S17B). Pharmacokinetic studies were performed in BT40 patient-derived xenograft (PDX) mice. Sampling was performed across a 24 h time window (Figure 5A) in both single-dose (Figure 5B) and multiple-dose (Figure 5C) cohorts.<sup>35</sup> Plasma concentration-time profiles for the cohorts are shown in Figure 5D, and pharmacokinetic parameters in Table 1. Total ulixertinib concentrations in the brain were measured using tissue homogenates of healthy brain and tumor regions (tumor, cerebellum, cortex/other brain regions) (Figure 5D). Ulixertinib disposition was comparable for malignant and healthy brain tissues. Ulixertinib showed low penetration of the blood–brain barrier with a brain disposition of 1.76% compared to plasma. Nevertheless,

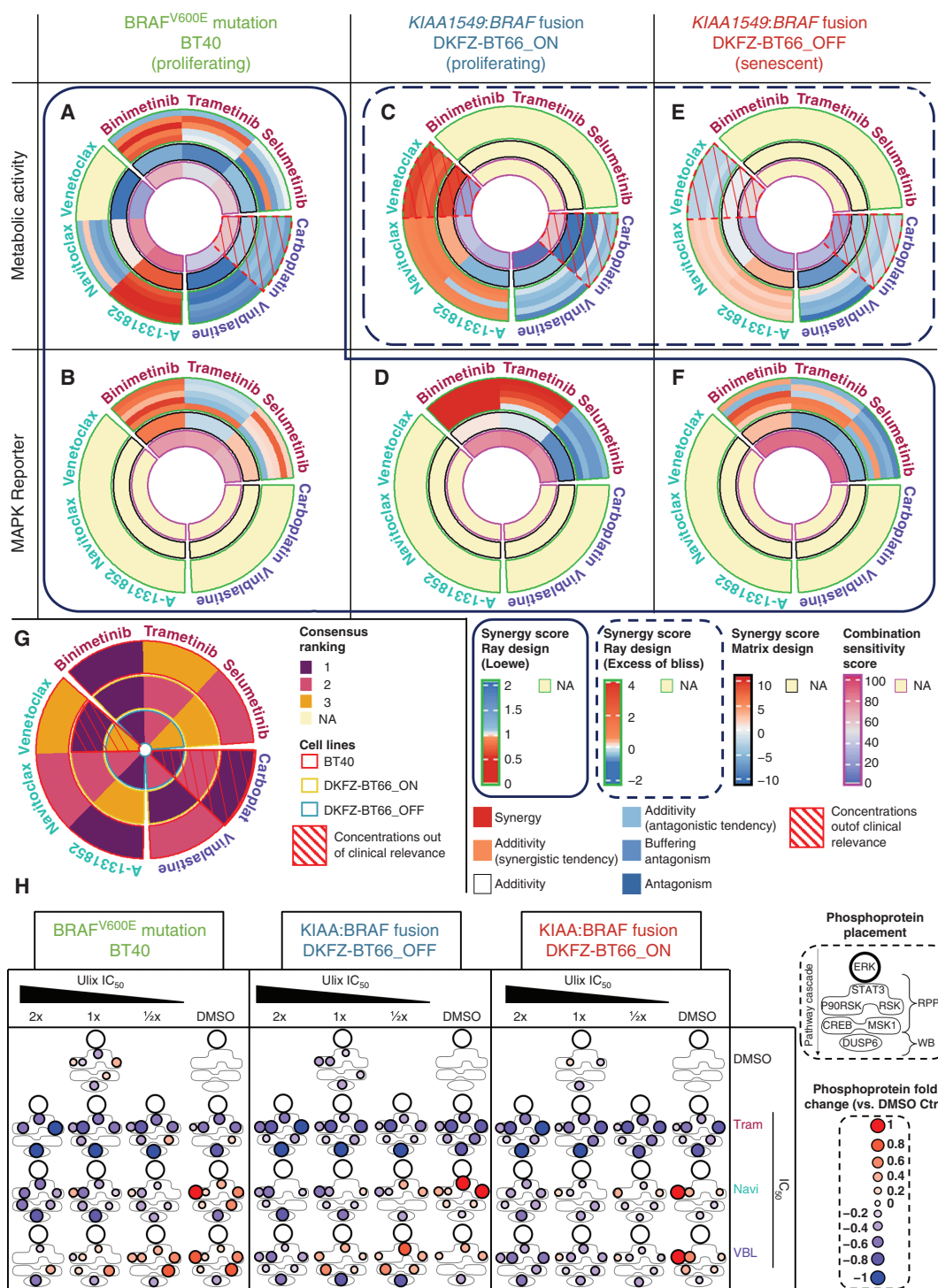


**Fig. 2** Synergy analysis and on-target activity of ulixertinib in combination with MEKi, BH3-mimetics, or chemotherapy. (A–F) Circular heatmaps summarizing the synergy results obtained in the tested combinations. Outermost ring: synergy scores of each ray; intermediate ring: average synergy score from the matrix design; innermost ring: combination sensitivity score from the matrix design. NA: synergy calculation not applicable. (G) Consensus ranking of the drugs across synergy metrics and across drugs for each drug class. (H) Miniaturized signaling network based on ERK downstream cascade (direct downstream targets: STAT3, P90RSK, RSK; nuclear targets: CREB, MSK1; downstream regulated protein: DUSP6). Protein phosphorylation fold-change in treated cells relative to the DMSO control is depicted.

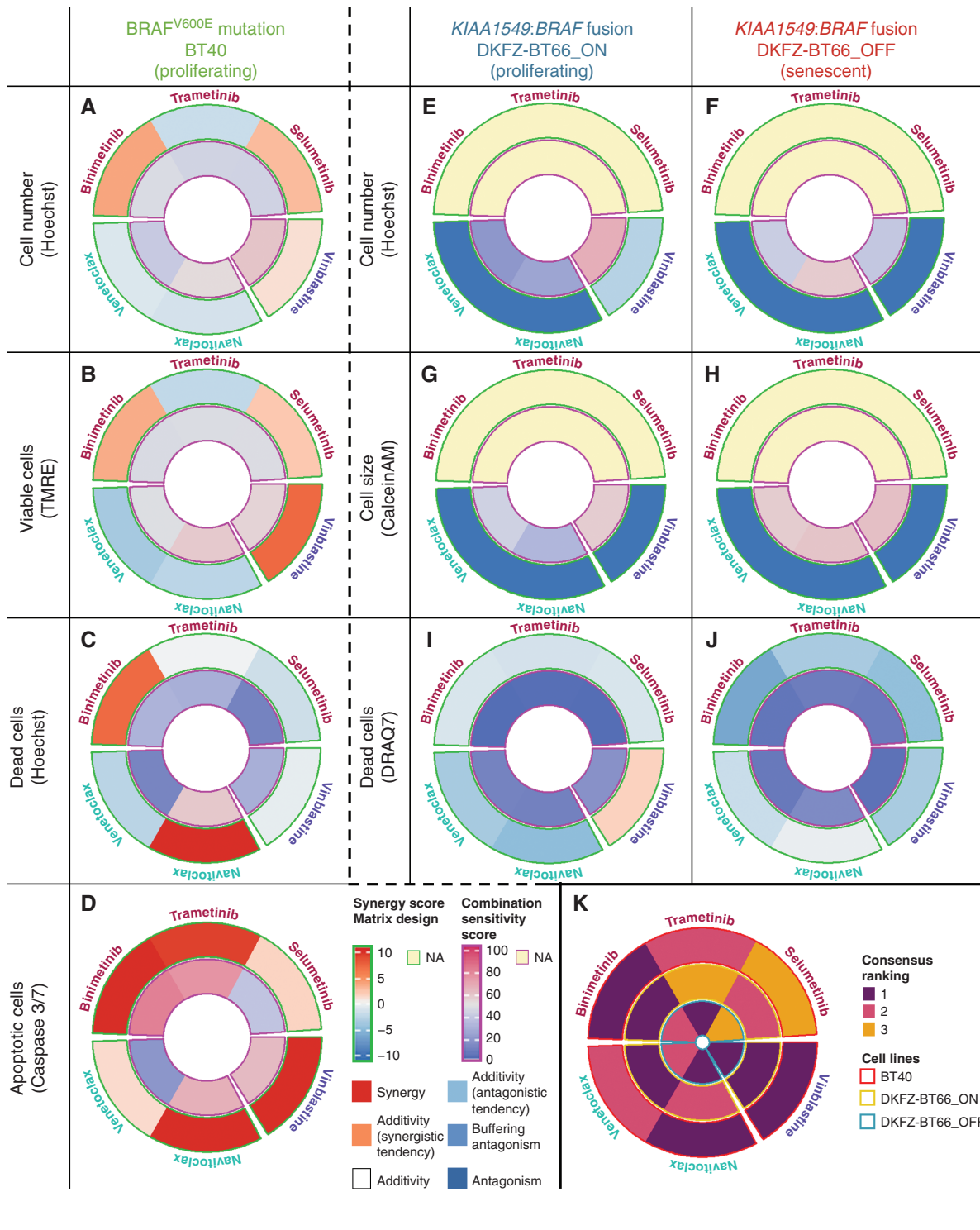


**Fig. 3** High content microscopy validation. (A–J) Circular heatmaps summarizing the synergy results obtained in the tested combinations via high content microscopy. Outermost ring: Synergy scores; innermost ring: combination sensitivity scores. NA, synergy calculation not applicable. (K) Consensus ranking of (A–J).

ulixertinib brain total concentrations exceeded effective in vitro IC<sub>50</sub> concentrations (30.4 ng/g) over the first 12 h after dosage in both cohorts. Hence, potentially effective brain concentrations were reached at steady-state.

To validate this, ulixertinib in vivo on-target activity was investigated by Western blot, in both healthy and tumor tissue from both treatment cohorts. Ulixertinib treatment induced a time-dependent inhibition of the DUSP6 protein,

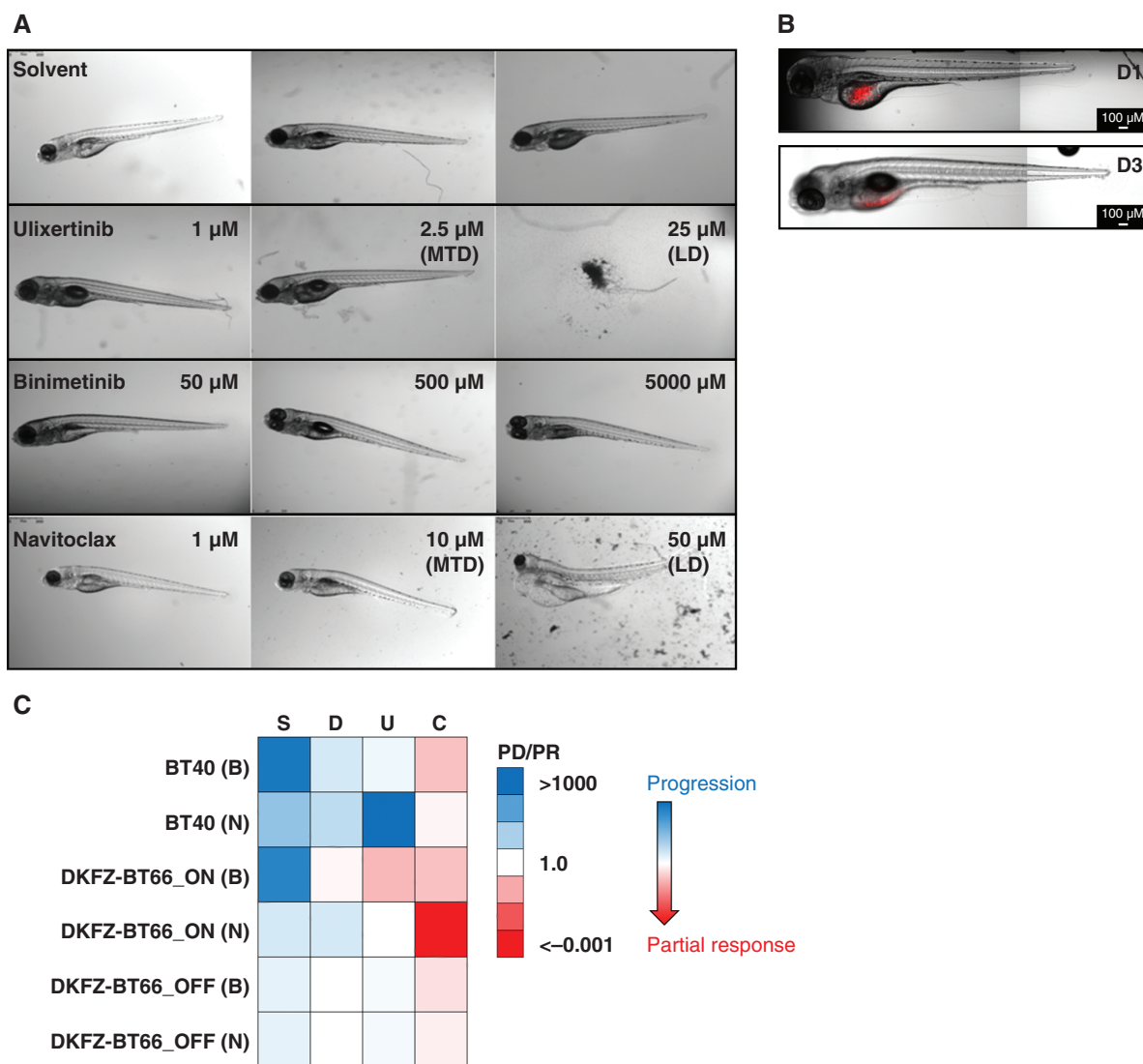


**Fig. 4** Zebrafish validation. (A) Representative exemplary pictures used to evaluate toxicity for ulixertinib, binimetinib, navitoclax, and DMSO, 72 h after treatment. MTD, maximal tolerated dose; LD, lethal dose. (B) Exemplary pictures of zebrafish embryo tumor transplantation. The scale bar represents 100  $\mu$ m. (C) Heatmap displaying the ratio of progressive disease (PD) to partial regression (PR) according to RECIST 1.1 adopted for zebrafish, using log<sub>10</sub> transformed values. S, solvent; D, drug of interest; U, ulixertinib; C, combination of ulixertinib and the drug of interest. (B) or (N): drug of interest, either binimetinib (B) or navitoclax (N).

correlating with the measured total drug tissue concentration (Supplementary Figure S18). No difference was observed between malignant and healthy brain tissue.

#### Ulixertinib Treatment Demonstrates Antitumoral Efficacy In Vivo in a Murine Orthotopic pLGG Model

Treatment with the indicated drugs was started 2 weeks posttransplantation, aiming to complete the treatment period of 19 days within the average 35.5 days latency of the model (Figure 5E). Ulixertinib exhibited a significant antitumoral activity in the PDX mouse model

(Figure 5F), and slowed down tumor growth (log-rank test,  $P = .0019$ ) with a median survival of 48.5 days in treated mice versus 30 days in mice receiving the vehicle (Figure 5G). Neither navitoclax nor vinblastine in combination with ulixertinib (log-rank test,  $P = .1939$  and  $P = .5551$ , respectively compared to ulixertinib treatment) significantly improved this outcome (Figure 5G). We measured navitoclax concentration in the tumor tissue and found that only 3/6 mice in the navitoclax monotherapy group, and 1/6 mice in the combination group showed tumor tissue concentrations above the effective in vitro navitoclax IC<sub>50</sub> (Supplementary Table S7), possibly explaining the low efficiency observed in the groups treated with navitoclax.

**Table 1** Single and Multiple Dose Pharmacokinetics of Oral Administration of Ulixertinib in NSG Mice

Cohort	Dose (mg/kg)	$C_{max}$ ( $\mu\text{g/ml}$ )	$t_{max}$ (h)	$AUC_{tot}$ ( $\mu\text{g/ml}\times\text{h}$ )	%AUC <sub>extra</sub>	$t_{1/2}$ (h)	$V_{ss}/F$ (L)	$Cl/F$ (ml/min)	$Cl/F \times F_{brain}$ (ml*min)	$V_{ss}/F \times F_{brain}$ (L)	$F_{brain}$ (%)
Single-dose plasma	80	7.52	2	64.6	2.03	4.14	0.188	0.477			
Multiple-dose plasma	80	10.9	2	76.3	0.401	2.88	0.121	0.404			
Multiple-dose brain	80	0.40	2	1.40	4.08	5.67	8.95	22.1	0.421	0.171	1.76

**Abbreviations:** AUC, area under the concentration–time curve;  $C_{max}$ , maximal plasma concentration;  $Cl/F$ , apparent clearance;  $F$ , bioavailability;  $t_{max}$ , time of maximal plasma concentration;  $t_{1/2}$ , half-life;  $V_{ss}/F$ , apparent volume of distribution.

Of note, pertaining tumor growth inhibition, ulixertinib outperformed the SOC chemotherapy (vinblastine) (Figure 5G and Supplementary Figure S19). However, after termination of the treatment, tumor growth accelerated in all survivors, highlighting ulixertinib's cytostatic activity (Figure 5F and Supplementary Figure S19). While all therapies were generally well tolerated, some of the mice treated with navitoclax or vinblastine experienced a minor weight loss (<20%), independent of brain tumor-related symptoms (Supplementary Figure S20).

## Discussion

Preclinical testing of novel drug candidates represents a necessary prerequisite for the development of new clinical trials. It allows to 1) assess their clinical potential, since drugs targeting the same pathway or belonging to the same class do not always have the same potency on a given model,<sup>23</sup> and 2) anticipate potential unexpected undesirable effects. For instance, the multi-kinase (including BRAF) inhibitor sorafenib, was thought to be beneficial for the treatment of BRAF-driven low-grade astrocytomas, based on their driving BRAF alterations. But its clinical evaluation in a phase II study demonstrated an unexpected tumor growth acceleration, later explained in vitro by paradoxical MAPK pathway activation.<sup>36</sup>

We here provide the first preclinical data describing the antitumoral activity of the first-in-class ERKi ulixertinib in BRAF-driven pLGG models. It showed a remarkable potency in the BRAF<sup>V600E</sup> (BT40) model. Although no metabolic activity-related effects could be observed in the DKFZ-BT66 model, as previously described,<sup>10,23</sup> ulixertinib showed comparable potency on MAPK pathway activity in the BRAF-fusion models, both DKFZ-BT66\_ON, previously characterized as reflecting patients with high risk of progression, and DKFZ-BT66\_OFF, reflecting patients with low risk of progression.<sup>10</sup> The significant MAPK inhibition observed in proliferating and senescent models suggests that ulixertinib might be equally potent in both stable and progressive pLGG. In addition, ulixertinib's strong potency at clinically achievable concentrations suggests a promising therapeutic window for the treatment of pLGG. Importantly, no paradoxical MAPK activation consequent to ERK-related negative feedback loop inhibition was observed.

Our in vivo studies confirmed the good tolerability of ulixertinib at effective and clinically relevant concentrations, and presented a pharmacokinetic profile consistent with previously published human phase I pharmacokinetic data.<sup>20</sup> We demonstrated its effective brain penetration, reaching concentrations sufficient to induce MAPK pathway inhibition, in line with its CNS activity previously demonstrated clinically in glioblastoma multiforme and brain metastases.<sup>20</sup> Ulixertinib disposition in healthy and tumor tissue was similar, highlighting its ability to cross an intact BBB in a limited but efficient manner. Indeed, the achieved tissue concentrations were above the in vitro  $IC_{50}$ , which efficacy was confirmed by its inhibitory effect on the MAPK pathway's surrogate marker DUSP6. In fact, ulixertinib, a catalytic ERKi, is a potent inhibitor of ERK

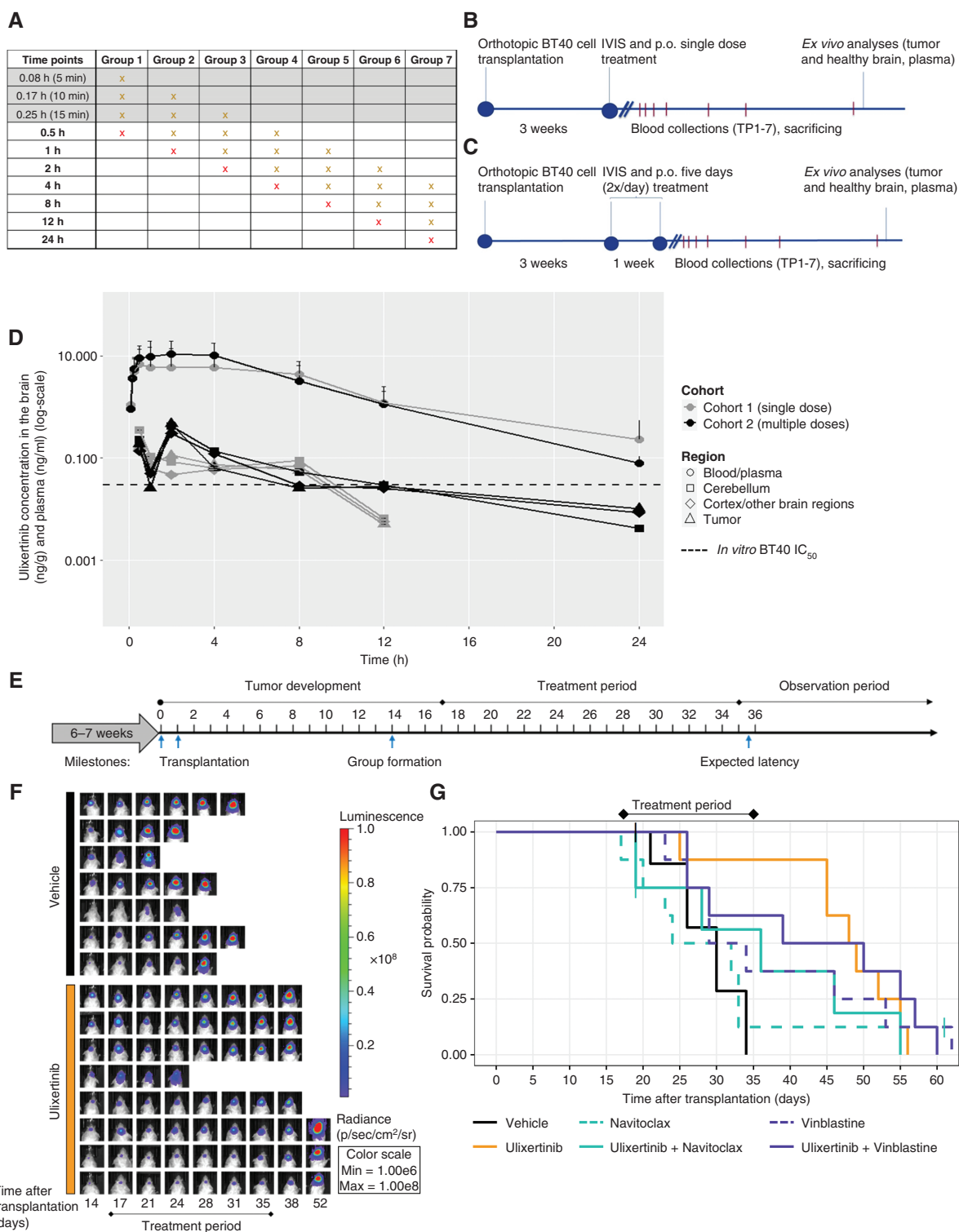


**Fig. 5** Pharmacokinetics data and preclinical evaluation of ulixertinib in vivo. (A) Blood collections of groups 1–7 for both dosing cohorts (single and multiple dose 2x/day, five days). Pivotal timepoints were defined for 0.5–24 h (indicated in bold). Three blood collections and one additional terminal collection via cardiac puncture were performed per mouse. (B–C) Study design of the ulixertinib pharmacokinetic experiment. (D) Ulixertinib plasma and brain concentrations in the single dose and multiple dose cohort. (E) Timeline of the study design. (F) Bioluminescence images of treated mice. Animals were imaged twice per week until reaching termination criteria. Bioluminescence signals are depicted as average radiance in the range of 1.0E6–1.0E8 photons/s/cm<sup>2</sup>/steradian. (G) Kaplan–Meier survival analysis of all treated animals as indicated ( $n = 8$  per group). Censored animals were sacrificed because of brain tumor independent reasons.

kinase activity, but not of its phosphorylation by upstream MEK, making phospho-ERK impossible to use to assess ulixertinib's MAPK inhibition efficacy.<sup>21</sup> MAPK downstream effectors were therefore suggested as reliable surrogates of MAPK activity to assess ulixertinib effects.<sup>22</sup> DUSP6 protein expression has been described as an accurate marker of elevated RAF/MEK/ERK pathway output in several MAPK-driven cell lines.<sup>37,38</sup> Indeed, Germann et al. have confirmed that quantifying MAPK downstream targets (i.e. DUSP6) was a reliable pharmacodynamic biomarker for ulixertinib-mediated inhibition of ERK1/2 activity.<sup>22</sup> While the effects on the tumor tissue led to tumor stabilization and prolonged survival, its effects on the normal tissue did not impair the well-being of the mice, as estimated by weight loss, behavior, and grooming routine monitoring. To our knowledge, our study is the first to provide an in-depth pharmacokinetic and pharmacodynamic analysis of ulixertinib brain tissue penetrance and activity in an in vivo model.

Ulixertinib delayed tumor growth and led to a significant survival increase in our BT40-PDX mouse model, probably via induction of cell death, as demonstrated in our study in vitro, and already observed in vivo at similar concentrations in KRAS-driven tumor xenografts.<sup>39</sup> This response pattern in vivo is similar to the one observed in a preclinical evaluation of the type 2 BRAFi tovorafenib (DAY101) in orthotopic mouse models (BRAF<sup>V600E</sup>- and *KIAA1549:BRAF*-transduced p53<sup>-/-</sup> neuro-progenitor cells),<sup>40</sup> which has since shown promising antitumor activity in a phase I study.<sup>41</sup> In terms of survival, ulixertinib outperformed chemotherapy during treatment, consistent with another preclinical study showing its significant survival benefit over chemotherapy (temozolomide) in a BRAF<sup>V600E</sup>-driven melanoma A375-PDX mouse model.<sup>22</sup> Taken together, our in vivo findings are suggestive of strong clinical significance of ulixertinib in BRAF-driven pLGG, and will support its first clinical evaluation as mono- and combination-therapy in pLGG in a currently planned international phase I/II umbrella trial.

Several drugs have been investigated as putative combination partners for ulixertinib, such as inhibitors of HER/ErbB, PI3K, and hydroxychloroquine.<sup>39,42,43</sup> However, only few combinations are currently under clinical investigation, for example with palbociclib in advanced pancreatic and other tumors (NCT03454035), and with hydroxychloroquine in gastrointestinal adenocarcinomas (NCT04145297). Here, we established a unique multi-layered integrated combination screen to identify clinically relevant combination partners for ulixertinib for the treatment of BRAF-driven pLGG. A limitation of this pipeline was the amount of pLGG models used. As has been discussed extensively/previously in the literature, the lack of reliable pLGG models remains a major drawback to date, with current cellular models not fully recapitulating the true pLGG biology.<sup>44</sup> An alternative is the use of primary patient-derived models, however strictly limited by their low proliferation rate, preventing their use in large scale screening pipeline. The DKFZ-BT66 remains the only model to date capable of transiently increasing its proliferation via the inducible expression of the SV40 large T antigen (DKFZ-BT66\_ON)

allowing their expansion, while still recapitulating the true biology of pLGG, in particular when repressing the expression of the SV40 large T antigen (DKFZ-BT66\_OFF) after expansion.<sup>10</sup> Hence, together with the pleomorphic xanthoastrocytoma-derived model BT40, they represent the only proliferating pLGG cell models usable on a large scale for such screens.

A first efficient combination partner for ulixertinib was recently demonstrated by a study in pancreatic cancer models showing moderate to strong synergism of ulixertinib combined with chemotherapy (gemcitabine) in vitro, and strong synergism in tumor volume reduction in vivo.<sup>39</sup> In our study, the combination of ulixertinib with vinblastine showed moderate synergy in vitro, and was moderately more beneficial for survival compared to vinblastine alone in vivo, potentially indicating clinical relevance.

German et al. have demonstrated strong synergistic activity of ulixertinib in combination with BRAFi (dabrafenib) in a BRAF<sup>V600E</sup>-mutant melanoma model in vivo.<sup>22</sup> We have previously published the first data on synergistic suppression of MAPK activity by the combination of type I or II BRAFi and ERKi in pLGG models in vitro, including ulixertinib and the second-generation type I BRAFi encorafenib.<sup>23</sup> It has also been shown that the coinhibition of both ERK and MEK resulted in extensive and durable suppression of MAPK activity, showing synergistic effects in KRAS-driven PDAC and NSCLC models in vivo.<sup>45</sup> Here, combinations of the ERKi ulixertinib with MEKi showed promising results. In particular, the MEKi binimetinib consistently topped the synergy rankings in the in vitro screens and showed antitumoral potential in combination with ulixertinib in the zebrafish embryo model. Interestingly, selumetinib in combination with ulixertinib showed indications for synergy in the BRAF<sup>V600E</sup> mutant model, but only additive effects in the *KIAA1549:BRAF*-fusion model. This suggests that the combination of ulixertinib with selumetinib might have a therapeutic benefit in BRAF<sup>V600E</sup> pLGG, which is of high clinical interest since the PFS upon treatment with selumetinib monotherapy is lower in pLGG with BRAF<sup>V600E</sup> compared to *KIAA1549:BRAF*-fusion.<sup>11</sup> It is important to note however that a recent phase Ib study, evaluating the combination of the MEKi cobimetinib with the ERKi GDC-0994 in adult, showed limited tolerability.<sup>46</sup>

Finally, strong synergism of ulixertinib with the BH3-mimetic S63845 (MCL-1 inhibitor) was recently demonstrated in rhabdomyosarcoma cells in vitro.<sup>47</sup> We demonstrated clear synergy of ulixertinib with BH3-mimetics in all BRAF-driven pLGG models. Navitoclax consistently showed synergism with ulixertinib in vitro, and the highest partial remission rate in zebrafish embryo models, while moderately exceeding the effects of navitoclax alone in the in vivo mouse model. This last observation could be explained by insufficient blood-brain barrier penetration of navitoclax, suggested by measured tumor concentrations below potentially effective values, in line with already published data.<sup>48-50</sup> Importantly, the Bcl-xL inhibitor A-1331852 showed the highest synergy scores across all models in the metabolic activity screen in vitro. Encouraging preclinical evidence supports the use of BH3-mimetics to target oncogene- and therapy-induced

senescent cells.<sup>24,25</sup> The use of Bcl-xL inhibitors could therefore represent a promising approach to be evaluated for pLGG treatment.

In conclusion, our data demonstrate the clinical relevance of the ERKi ulixertinib for the treatment of BRAF-driven pLGG, and will support its first clinical evaluation as single agent and in combination in a phase I/II combination umbrella trial in relapsed pLGG.

## Supplementary Material

Supplementary material is available at *Neuro-Oncology* online.

## Keywords

BH3-mimetics | ERK inhibitor | MAPK inhibitor | pediatric low-grade glioma | synergism

## Funding

This study was supported by BioMed Valley Discoveries; the Brain Tumor Charity -The Everest Centre for Low-Grade Pediatric Brain Tumours (GN-000382 to T.M., D.T.W.J. and O.W.); the Deutsche Konsortium für Translationale Krebsforschung (DKTK JF Upgrade Next Gen LOGGIC to T.M., I.O., and O.W.); the Deutsche Forschungsgemeinschaft (404521405 SFB 1389 to M.S., K.I.F., J.B. and W.E.H., INST 110489/51-1 FUGG to O.W.); the Ministry for Science and Culture of the State of Baden-Württemberg (AZ 41-4710 to S.M.P.).

## Acknowledgments

We thank Clarissa Holitsch, Alexandra Stroh-Dege, Aileen Mangang, Natalie Stumpf, Lea Hofmann, Laura Dörner and Anna Laudat for excellent technical support. We wish to thank Karen Frese and Benjamin Meder for their valuable support with the breeding and husbandry of the zebrafish.

**Conflict of interest statement.** C.M. van Tilburg participated in advisory boards of Novartis and Bayer. S.M. Pfister reports grants from the ITCC-P4 IMI-2 project funded by the EU as well as 10 EFPIA companies ([www.itccp4.eu](http://www.itccp4.eu)) outside the submitted work; S.M. Pfister has a patent for EP 16710700 A 20160311 (methylation-based tumor classification) issued. T. Milde and O. Witt received research funding from Biomed Valley and Day One Therapeutics. O. Witt has received research grants from BMS, Syndax and served as advisory board member for Novartis, Janssen, BMS, Bayer, Astra Zeneca.

## Author contributions

**Conceptualization:** T.M., O.W., I.O., M.Z., K.W.P., M.S., B.K., D.K., D.T.W.J., R.S., L.R., C.G., J.B., L.v.S. **Acquisition of data:** R.S., L.R., C.G., J.B., L.v.S., H.P., F.S., S.N., S.A., N.H., I.B., L.S., K.I.F., J.B., M.S. **Analysis and interpretation of data:** R.S., L.R., C.G., J.B., L.v.S., H.P., S.N., S.A., X.F.G., K.I.F., J.B., W.E.H., D.K., B.K., M.S., K.W.P., M.Z., I.O., O.W., T.M. **Writing, editing:** R.S., T.M., L.R., C.G., J.B., L.v.S., O.W., I.O., M.Z., K.W.P., M.S. **Reviewing:** All authors.

## References

1. Miller KD, Ostrom QT, Kruchko C, et al. Brain and other central nervous system tumor statistics, 2021. *CA Cancer J Clin.* 2021; 71(5):381–406.
2. Armstrong GT, Conklin HM, Huang S, et al. Survival and long-term health and cognitive outcomes after low-grade glioma. *Neuro Oncol.* 2011; 13(2):223–234.
3. De Blank P, Bandopadhyay P, Haas-Kogan D, Fouladi M, Fangusaro J. Management of pediatric low-grade glioma. *Curr Opin Pediatr.* 2019; 31(1):21–27.
4. Gnekow AK, Walker DA, Kandels D, et al. A European randomised controlled trial of the addition of etoposide to standard vincristine and carboplatin induction as part of an 18-month treatment programme for childhood ( $\leq 16$  years) low grade glioma—a final report. *Eur J Cancer.* 2017; 81:206–225.
5. Lassaletta A, Scheinemann K, Zelcer SM, et al. Phase II weekly vinblastine for chemotherapy-naïve children with progressive low-grade glioma: a Canadian pediatric brain tumor consortium study. *J Clin Oncol.* 2016; 34(29):3537–3543.
6. Milde T, Rodriguez FJ, Barnholtz-Sloan JS, et al. Reimagining pilocytic astrocytomas in the context of pediatric low-grade gliomas. *Neuro Oncology.* 2021; 23(10):1634–1646.
7. Jones DTW, Kocalkowski S, Liu L, et al. Tandem duplication producing a novel oncogenic BRAF fusion gene defines the majority of pilocytic astrocytomas. *Cancer Res.* 2008; 68(21):8673.
8. Jones DTW, Hutter B, Jäger N, et al. Recurrent somatic alterations of FGFR1 and NTRK2 in pilocytic astrocytoma. *Nat Genet.* 2013; 45(8):927–932.
9. Jones DTW, Gronych J, Lichter P, Witt O, Pfister SM. MAPK pathway activation in pilocytic astrocytoma. *Cell Mol Life Sci.* 2012; 69(11):1799.
10. Selt F, Hohloch J, Hielscher T, et al. Establishment and application of a novel patient-derived KIAA1549:BRAF-driven pediatric pilocytic astrocytoma model for preclinical drug testing. *Oncotarget.* 2017; 8(7):11460–11479.
11. Fangusaro J, Onar-Thomas A, Poussaint T, et al. Selumetinib in children with BRAF-aberrant or neurofibromatosis type 1-associated recurrent, refractory or progressive low-grade glioma: a multi-center phase II trial. *Lancet Oncol.* 2019; 20(7):1011.
12. Robison N, Pauly J, Malvar J, et al. LGG-52. Binimetinib in children with progressive or recurrent low-grade glioma not associated with neurofibromatosis type 1: initial results from a multi-institutional phase II study. *Neuro Oncology.* 2020; 22(Suppl 3):iii376.
13. Nobre L, Zapotocky M, Ramaswamy V, et al. Outcomes of BRAF V600E pediatric gliomas treated with targeted BRAF inhibition. *JCO Precis Oncol.* 2020; 13(4):561–571.

14. Nicolaidis T, Nazemi KJ, Crawford J, et al. Phase I study of vemurafenib in children with recurrent or progressive BRAFV600E mutant brain tumors: Pacific Pediatric Neuro-Oncology Consortium study (PNOC-002). *Oncotarget*. 2020; 11(21):1942–1952.
15. Selt F, Tilburg CM van, Bison B, et al. Response to trametinib treatment in progressive pediatric low-grade glioma patients. *J Neurooncol*. 2020; 149(3):499.
16. Dhillon AS, Hagan S, Rath O, Kolch W. MAP kinase signalling pathways in cancer. *Oncogene*. 2007; 26(22):3279–3290.
17. Yoon S, Seger R. The extracellular signal-regulated kinase: multiple substrates regulate diverse cellular functions. *Growth Factors*. 2009; 24(1):21–44.
18. Wortzel I, Seger R. The ERK cascade: distinct functions within various subcellular organelles. *Genes Cancer*. 2011; 2(3):195–209.
19. Sturm OE, Orton R, Grindlay J, et al. The mammalian MAPK/ERK pathway exhibits properties of a negative feedback amplifier. *Sci Signal*. 2010; 3(153):ra90.
20. Sullivan RJ, Infante JR, Janku F, et al. First-in-class ERK1/2 inhibitor ulixertinib (BVD-523) in patients with MAPK mutant advanced solid tumors: results of a phase I dose-escalation and expansion study. *Cancer Discov*. 2018; 8(2):184–195.
21. Kidger AM, Munck JM, Saini HK, et al. Dual-mechanism ERK1/2 inhibitors exploit a distinct binding mode to block phosphorylation and nuclear accumulation of ERK1/2. *Mol Cancer Ther*. 2020; 19(2):525–539.
22. Germann UA, Furey BF, Markland W, et al. Targeting the MAPK signaling pathway in cancer: promising preclinical activity with the novel selective ERK1/2 inhibitor BVD-523 (ulixertinib). *Mol Cancer Ther*. 2017; 16(11):2351–2363.
23. Usta D, Sigaud R, Buhl JL, et al. A cell-based MAPK reporter assay reveals synergistic MAPK pathway activity suppression by MAPK inhibitor combination in BRAF-driven pediatric low-grade glioma cells. *Mol Cancer Ther*. 2020; 19(8):1736–1750.
24. Buhl JL, Selt F, Hielscher T, et al. The senescence-associated secretory phenotype mediates oncogene-induced senescence in pediatric pilocytic astrocytoma. *Clin Cancer Res*. 2019; 25(6):1851–1866.
25. Guiho R, Selt F, Stone T, et al. LGG-09. Senolytic agent navitoclax targets vinblastine- and MAPK inhibitors-induced senescent tumour cells in paediatric low grade gliomas. *Neuro Oncol*. 2021; 23(Suppl 1):i33.
26. Kolb EA, Gorlick R, Houghton PJ, et al. Initial testing (stage 1) of AZD6244 (ARRY-142886) by the pediatric preclinical testing program. *Pediatr Blood Cancer*. 2010; 55(4):668–677.
27. McQuin C, Goodman A, Chernyshev V, et al. CellProfiler 3.0: next-generation image processing for biology. *PLoS Biol*. 2018; 16(7):e2005970.
28. Straetemans R, O'Brien T, Wouters L, et al. Design and analysis of drug combination experiments. *Biom J*. 2005; 47(3):299–308. doi:10.1002/bimj.200410124.
29. Zheng S, Wang W, Aldahdooh J, et al. SynergyFinder Plus: towards a better interpretation and annotation of drug combination screening datasets. *Genom Proteom Bioinform*. 2022; S1672-0229(22)00008-0. doi:10.1016/j.gpb.2022.01.004
30. Pierobon M, Robert NJ, Northfelt DW, et al. Multi-omic molecular profiling guide's efficacious treatment selection in refractory metastatic breast cancer: a prospective phase II clinical trial. *Mol Oncol*. 2022; 16(1):104–115.
31. Jameson GS, Petricoin EF, Sachdev J, et al. A pilot study utilizing multi-omic molecular profiling to find potential targets and select individualized treatments for patients with previously treated metastatic breast cancer. *Breast Cancer Res Treat*. 2014; 147(3):579–588.
32. Wrobel JK, Najafi S, Ayhan S, et al. Rapid in vivo validation of HDAC inhibitor-based treatments in neuroblastoma zebrafish xenografts. *Pharmaceuticals*. 2020; 13(11):3451–3420.
33. Yang W, Soares J, Greninger P, et al. Genomics of Drug Sensitivity in Cancer (GDSC): a resource for therapeutic biomarker discovery in cancer cells. *Nucleic Acids Res*. 2013; 41(D1):D955–D961.
34. Lazzareschi I, Ruggiero A, Riccardi R, et al. Hypersensitivity reactions to carboplatin in children. *J Neuro-Oncol*. 2002; 58(1):33–37.
35. Suresh PS, Jairam RK, Chandrasekhar DV, et al. Prediction of human pharmacokinetics of ulixertinib, a novel ERK1/2 inhibitor from mice, rats, and dogs pharmacokinetics. *Eur J Drug Metab Pharmacokinet*. 2018; 43(4):453–460.
36. Karajannis MA, Legault G, Fisher MJ, et al. Phase II study of sorafenib in children with recurrent or progressive low-grade astrocytomas. *Neuro Oncol*. 2014; 16(10):1408.
37. Pratilas CA, Taylor BS, Ye Q, et al. V600EBRAF is associated with disabled feedback inhibition of RAF–MEK signaling and elevated transcriptional output of the pathway. *Proc Natl Acad Sci*. 2009; 106(11):4519–4524.
38. Buffet C, Hecale-Perlemoine K, Bricaire L, et al. DUSP5 and DUSP6, two ERK specific phosphatases, are markers of a higher MAPK signaling activation in BRAF mutated thyroid cancers. *PLoS One*. 2017; 12(9):e0184861.
39. Jiang H, Xu M, Li L, et al. Concurrent HER or PI3K inhibition potentiates the anti-tumor effect of ERK inhibitor ulixertinib in preclinical pancreatic cancer models. *Mol Cancer Ther*. 2018; 17(10):2144.
40. Sun Y, Alberta JA, Pilarz C, et al. A brain-penetrant RAF dimer antagonist for the noncanonical BRAF oncoprotein of pediatric low-grade astrocytomas. *Neuro Oncol*. 2017; 19(6):774–785.
41. Wright K, Krzykwa E, Greenspan L, et al. EPCT-01. Phase I study of day101 (TAK580) in children and young adults with radiographically recurrent or progressive low-grade glioma (LGG). *Neuro Oncol*. 2020; 22(Suppl 3):iii304–iii304.
42. Hayes TK, Neel NF, Hu C, et al. Long-term ERK inhibition in KRAS-mutant pancreatic cancer is associated with MYC degradation and senescence-like growth suppression. *Cancer Cell*. 2016; 29(1):75–89.
43. Bryant KL, Stalneck CA, Zeitouni D, et al. Combination of ERK and autophagy inhibition as a treatment approach for pancreatic cancer. *Nat Med*. 2019; 25(4):628–640.
44. Chiacchiarini M, Besharat ZM, Carai A, et al. Pediatric low-grade gliomas: molecular characterization of patient-derived cellular models. *Child's Nerv Syst*. 2021; 37(3):771–778.
45. Merchant M, Moffat J, Schaefer G, et al. Combined MEK and ERK inhibition overcomes therapy-mediated pathway reactivation in RAS mutant tumors. *PLoS One*. 2017; 12(10):e0185862.
46. Weekes C, Lockhart A, LoRusso P, et al. A phase Ib study to evaluate the MEK inhibitor cobimetinib in combination with the ERK1/2 inhibitor GDC-0994 in patients with advanced solid tumors. *Oncologist*. 2020; 25(10):833.
47. Winkler M, Friedrich J, Boedicker C, Dolgikh N. Co-targeting MCL-1 and ERK1/2 kinase induces mitochondrial apoptosis in rhabdomyosarcoma cells. *Transl Oncol*. 2022; 16:101313.
48. Yamaguchi R, Perkins G. Finding a panacea among combination cancer therapies. *Cancer Res*. 2012; 72(1):18–23.
49. Koessinger AL, Cloix C, Koessinger D, et al. Increased apoptotic sensitivity of glioblastoma enables therapeutic targeting by BH3-mimetics. *Cell Death Differ*. 2022; 1–16. doi:10.1038/s41418-022-01001-3
50. He W, Li X, Morsch M, et al. Brain-targeted codelivery of Bcl-2/Bcl-xl and Mcl-1 inhibitors by biomimetic nanoparticles for orthotopic glioblastoma therapy. *ACS Nano*. 2022; 16(4):6293–6308.